Physica E 126 (2021) 114446

Contents lists available at ScienceDirect

Physica E: Low-dimensional Systems and Nanostructures

journal homepage: http://www.elsevier.com/locate/physe

Promising two-dimensional nanocomposite for the anode of the lithium-ion batteries. Computer simulation

A.Y. Galashev [a,b,*], O.R. Rakhmanova [a,b]

[a] Institute of High-Temperature Electrochemistry, Ural Branch of Russian Academy of Sciences, Academicheskaya Str., 20, Yekaterinburg, 620990, Russia
[b] Ural Federal University named after the first President of Russia B.N. Yeltsin, Mira Str., 19, Yekaterinburg, 620002, Russia

ARTICLE INFO

Keywords:
Doped silicene channel
Graphite substrate
Lithium ion
Molecular dynamics
Stress distribution
Structure

ABSTRACT

To create a high-performance lithium-ion battery, a new anode material is needed. We study the structure, dynamics, and mechanical properties of a promising anode silicene/graphite material subjected to the transmutation neutron doping. The motion of the lithium ion under electric field along a silicene channel located on a graphite substrate was studied. The concentration of phosphorus in the walls of the silicene channel varied from 3% to 18%. The concentration of nitrogen in the graphite substrate was 5%. Both the gap and the amount of phosphorus in the channel walls were found to affect the movement of the lithium ion along the channel. As a rule, strong stresses in the silicene sheets are not observed during the movement of the Li^+ ion along the channel. The maximum values of local stresses arising in the walls of the channel turn out to be slightly sensitive both to the doping degree of silicene and to the size of the channel gap. The top sheet of the silicene channel always has a larger roughness than the bottom one. To use silicene in a lithium-ion battery, the maximum doping degree of silicene with phosphorus should not exceed 9%.

1. Introduction

The use of anode materials with layered structures leads to the creation of large adsorption surfaces. That help to achieve a significant charge capacity of the electrode [1]. Also, in such electrodes, the diffusion path becomes shorter and faster. This is important for obtaining a higher battery charge rate. Silicene is a 2D silicon structure with a buckled monoatomic layer. This is a silicon analog of graphene. Both in graphene and in silicene, electrons behave like massless fermions in the vicinity of the Dirac points [2]. The non-flat (i.e. bending) structure of silicene makes it more suitable than graphene for many applications [3]. Silicene has unique features such as the quantum spin Hall effect, large spin-orbit interaction and tunable band gap [4].

Due to sp^2-hybridization and dangling edge bonds, self-standing silicene has low stability and, probably, cannot exist without a substrate [5]. The stability of silicene increases with increasing number of layers [6]. The bilayer silicene on the graphite substrate formed from graphene sheets is a stable structure. It is resistant to lithiation/delithiation processes, even in the presence of the large number of vacancies [7]. A certain affinity between the structures of silicene and graphene plays an important role here.

The silicene surface can be easily functionalized [8]. The necessary mechanical and electronic properties of the silicene structure can be tuned by doping. Various techniques could be used for doping of silicon: rapid-thermal diffusion from spin-on doping sources [9], accelerated diffusion of phosphorus in a single crystal of silicon, which takes place during the decomposition of the over-saturated inhomogeneous solid solution [10], low-temperature molecular beam epitaxy [11], high-temperature ion implantation [12]. Unfortunately, neither technique produces a highly homogeneous dopant concentration. In addition, the ion implantation can result in the unwanted lattice defects in the semiconductor. The method of neutron transmutation doping has also become widespread [13]. The significant advantage of this approach is the possibility to control the amount of dopant and its uniform distribution over the initial material [14]. As a result of transmutation, phosphorus is formed from silicon, and nitrogen is formed from carbon.

The electronic properties of free-standing silicene doped with phosphorus, as well as the change in its shape, were considered in an *ab initio* study [8]. The silicene structure remains unbroken even at high temperatures because the bond between Si and P atoms is very strong. There is a significant change in the electronic structure of the hydrogenated

* Corresponding author. Institute of High-Temperature Electrochemistry, Ural Branch of Russian Academy of Sciences, Academicheskaya Str., 20, Yekaterinburg, 620990, Russia.
E-mail address: alexander-galashev@yandex.ru (A.Y. Galashev).

https://doi.org/10.1016/j.physe.2020.114446
Received 25 May 2020; Received in revised form 31 August 2020; Accepted 18 September 2020
Available online 7 October 2020

silicene when the phosphorus doping varies from 1.4% up to 12.5% [15]. Moreover, the higher the phosphorus concentration, the greater is the difference between the energies of the Fermi level and the maximum of the valence band (0.13–0.79 eV).

The future of silicene is associated with its possible integration into the efficient energy, mostly, development of a new generation of energy storage and autonomous devices such as lithium-ion batteries (LIBs). Silicon-based electrodes can have a specific capacity of up to 4200 mAh/g [16]. However, the use of bulk silicon in Li-ion batteries leads to its degradation during lithiation/delithiation cycles [17]. On the contrary, the use of a two-dimensional analog of silicon, silicene, can be promising for improving LIBs. Silicene has a large specific surface area, high mechanical flexibility, and electron mobility. So, it can be considered as a suitable material for LIB. The DFT calculations demonstrated that the theoretical specific capacity of a single-layer silicene anode is estimated as 954 mAh/g [18]. For a two-layer silicene anode, it has a value of 1384 mAh/g [17]. It is 2.5–3.7 times higher than that of graphite electrodes. Moreover, the structure of the silicene sheet does not degrade during lithiation and delithiation [19]. Not only lithium, but also sodium batteries can have a greater performance. For example, solid-state sodium batteries with Na_3PO_4 electrolyte are characterized by the increased safety and low-cost production [20].

Silicene is noticeably inferior in strength to graphene [21]. The tensile strength of silicene (23 GPa) is 5–6 times lower than that of graphene. When silicene with vacancy defects is used in the anode design (instead of perfect silicene), the high capacity values of the two-dimensional electrode are achieved [22,23]. The Si–P bond (~3.1 eV) is stronger than the Si–Si (~2.3 eV) and P–P ones (~2.09 eV). So, it can be expected that doping of silicene with phosphorus can strengthen the defective silicene [24]. It is of interest to find out, how promising is to use the phosphorus-doped two-layer silicene as the anode material of the new generation LIBs.

The present study is aimed at the investigation of the mechanism of the lithium ion motion along the flat open channel. The channel is formed by the phosphorus-doped silicene sheets and located on the nitrogen-doped graphite substrate. In addition, the study of the structure and mechanical properties of the channel walls as the lithium ion moves along the channel is also the goal of the present work.

2. Computational methodology

The calculations were performed using the classical molecular dynamics (MD) method. The interactions in the silicene sheets and graphite substrate were described by the Tersoff potential [25]. The parameters were taken from Ref. [26]. The Tersoff potential was successfully used for simulation of 2D systems [5,21–23,27]. It has a good transferability for bond orbitals. The parameters fitted to the sp^3-hybridization can be used to describe the interaction in materials with the sp^2-hybridization [28].

To test the suitability of the Tersoff potential for silicene modeling, we calculated the elastic properties of the single-layer perfect silicene using this potential. The elastic moduli of silicene were determined by applying a uniform deformation of a unit cell at T = 293 K. Two (C_{11} and C_{12}) of five (beside these C_{13}, C_{33}, and C_{44}) independent modules of a hexagonal structure are the most important. Because they correspond to the isotropic linear elasticity in the plane. The Young's modulus Y and Poisson's ratio ν, bulk modulus K and shear modulus G were determined in terms of the moduli C_{11} and C_{12} [29] according to

$$Y = \frac{(C_{11}^2 - C_{12}^2)}{C_{11}} \quad (1)$$

$$\nu = C_{12}/C_{11} \quad (2)$$

$$K = \frac{(C_{11} + 2C_{12})}{3} \quad (3)$$

$$G = \frac{(C_{11} - C_{12})}{2} \quad (4)$$

The calculated values of C_{11}, C_{12}, Y, ν, K, and G are presented in Table 1 together with the corresponding characteristics of silicene determined using the DFT calculations [30], as well as the characteristics of bulk silicon and graphene. Calculations for graphene were performed by the classical molecular dynamics method using the Tersoff potential [31].

As it can be seen from Table 1, the elastic moduli (C_{11} and C_{12}) and the Poisson's ratio calculated using the Tersoff potential are higher than the corresponding values determined by the DFT calculations [30]. It can also be noted, that silicene has higher elastic constants as well as bulk and shear modulus than bulk silicon. At the same time, in comparison with graphene, the shear modulus of silicene in the sheet plane and Young's modulus are 8.1 and 6.3 times lower, respectively, and Poisson's ratio, on the contrary, is 3.6 times higher. Consequently, silicene is much less stiff than graphene.

The interaction between the lithium ion and silicon and carbon atoms was described by the Morse potential [32] using parameters reported in Refs. [33,34]. The interactions inside the sheets of silicene and graphene with dopants (phosphorus and nitrogen, respectively) were taken into account using the Morse potential. The parameters of this potential were calculated in the DFT model according to the methodology reported in Ref. [35]. The obtained parameters of the potential are provided in Ref. [36]. The Lennard-Jones potential was used to describe the interactions between graphene sheets in the graphite substrate [37]. The experimental value of the distance r_{C-C} between the graphene sheets and the calculated value of the distance r_{Si-C} between silicene and the substrate obtained in quantum mechanical calculations [38,39] were reproduced in the present MD calculations.

The silicene sheet contained 300 Si atoms and had geometric sizes of 5.4 × 4.3 nm (Fig. 1). A unit cell of the defect-free sheet consisted of 18 silicon atoms. In this floral structure of the single-layer silicene, six atoms of a unit cell were located above the main plane at the distance of 0.074 nm. The silicene sheets were displaced (in the *xy* plane by 0.012 nm) relative to each other forming the Bernal stack (AB). When the distance between two parallel silicene sheets is sufficient for the movement of a lithium ion under the applied electric field, it can be considered that they form a silicene channel. In this case, we will refer to the silicene sheets as the channel walls. If there is a single Li^+ ion in the channel, it will spend most of the time near the channel walls. This is due to the presence of a molecular force field generated by Si atoms. All atoms of the system including the Li^+ ion are involved in the thermal movement. The interaction of the ion with the electric field is expressed in the presence of an additional force directed along the vector of the electric field strength. Usually, in the electric fields which are not so strong ($<10^6$ V/m), this force is small concerning the resulting force caused by the interatomic interaction.

The gap h_g between the silicene sheets varied from 0.60 to 0.80 nm. The lithium ion was initially placed at the entrance of the channel and was pushed into it. The lithium ion horizontal coordinates were: $x = 0.71$ nm, $y = 2.4$ nm. In this case, the Li^+ ion was located at an equal distance from the silicene sheets (channel walls), i.e. its *z* coordinate was $h_g/2$ when it is measured from the position of the lower silicene sheet.

Table 1
Elastic properties of perfect silicene, bulk silicon and graphene.

Elastic properties	C_{11} (GPa)	C_{12} (GPa)	Y (GPa)	ν	K (GPa)	G (GPa)
Perfect silicene (Tersoff)	215	97	171	0.45	136	59
Perfect silicene, DFT calculations [30]	204	66	182	0.325	112	69
Bulk silicon	166	64	179	0.278	98	52
Graphene MD calculations [31]	1094	136	1077	0.1248	455	479

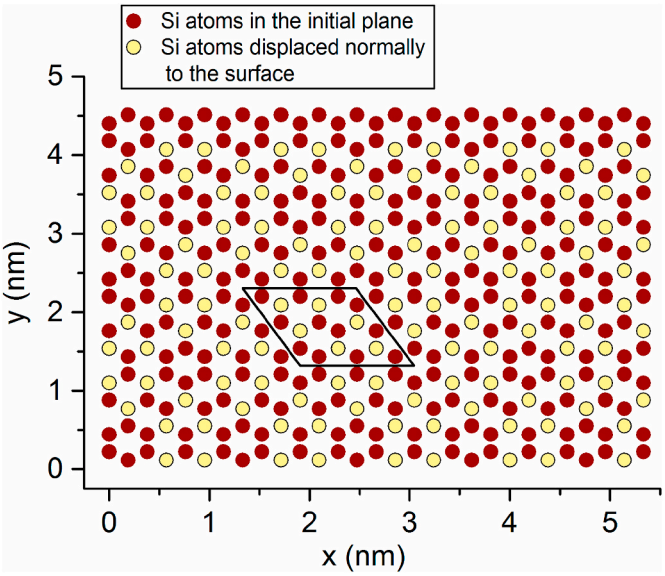

Fig. 1. Top view of the silicene structure at the initial instant; an outline shows a surface cell unit of the silicene sheet.

The edge Si atoms in the silicene sheets were fixed [40]. The intensity of the constant electric field applied to the system was 10^5 V/m. The direction of the field strength vector coincided with the 0*x* axis ("zig-zag" direction). Such field strength is observed in the electrolyte of a real thin-film LIB when the distance between electrodes is ~3 μm [41]. The time step Δt duration was $1{\cdot}10^{-16}$ s. The geometric optimization of the system over 10 000 time steps was performed. After that, the principal MD calculation began with a duration of 1 million time steps (100 ps) for each system. As a rule, this time was sufficient for the Li^+ ion to pass the silicene channel located on different substrates [42,43].

To form a doped silicene structure, 9 vacancy defects were created in each silicene sheet. Then they were filled with P atoms. In other words, missing Si atoms were replaced by P ones. The filling of nine monovacancies corresponded to 3% of the content of P element, bivacancies – 6%, trivacancies – 9%, and hexavacancies – 18% of the doping element.

Three graphene sheets were stacked (according to the Bernal stacking) to build a substrate on which the silicene channel was located. The distance between layers in the graphite substrate corresponded to the experimental data $r_{C-C} = 0.335$ nm [38]. The distance between the silicene channel and the substrate was $r_{Si-C} = 0.286$ nm, it was obtained from *ab initio* calculations [39]. All three layers of the substrate were doped with nitrogen atoms. The degree of doping was 5%. Previously, it was shown in the MD simulation, that the silicene channel modified by the vacancy defects and located on the graphite substrate appeared to be more stable to the lithiation/delithiation cycles than the silicene channel located on any other metal substrates [43]. Therefore, the graphite substrate is suitable for the lithiation of bilayer silicene.

The problems we solve in the framework of classical molecular dynamics have asymmetric boundary conditions. Periodic boundary conditions cannot be used here to expand the system. Therefore, the boundary conditions were free in all directions. The total size of the system was 3948 atoms, including 600 Si and P atoms in two doped silicene sheets, and 3348 C and N atoms in three doped graphene sheets forming a substrate. The size of the system could influence the time during which the lithium ion passes the silicene channel: the larger is the system, the longer it takes the Li^+ ion to pass the Si channel. However, the appearance of the vacancy defects in the channel walls (especially large ones, such as tri- and hexavacancies) reduces the influence of the size of the system to the time of the lithium ion passage through the silicene channel.

The calculations aimed at the study of the mechanism of the lithium ion transport along the doped silicene channel on the graphite substrate were performed in two stages. At the first stage, the doping degree of the silicene sheets was constant (3%), and the h_g gap size varied and corresponded to: $h_g = 0.6$, 0.7, 0.75, and 0.8 nm. These computational experiments allowed us to determine the effect of the gap size of the doped silicene channel on the speed of the lithium ion passage through the channel. At the second stage of the calculations, the gap size was constant ($h_g = 0.75$ nm), and the doping degree of the silicene sheets varied and corresponded to the following values: 3%, 6%, 9%, 18%. Analyzing the results of these calculations, we studied the effect of the phosphorus concentration on the transport properties of the lithium ion in the channel. Also, we evaluated the structural rearrangements in the silicene sheets. They were caused both by the movement of the ion and by the displacement of the P atoms from their initial locations.

Stresses arising in the silicene sheets of the systems under consideration were calculated by the method described in Refs. [44,45]. The virial stress can be represented by the virial theorem in the following form [46]:

$$\sigma_{u\alpha}^{V} = \frac{1}{V}\sum_{i}\left[\frac{1}{2}\sum_{j-1}^{N}\left(r_u^j - r_\alpha^i\right)f_\alpha^{ij} - n_d k_B T^i\right] \quad (5)$$

here (u, α) have *x, y, z* values of directions, $j = 1 \ldots N$ is the number of neighbors of the *i* atom under consideration, r_u^i is the location of the *i* atom in the direction *u*, f_α^{ij} is the force acting on the *i* atom from the side of the *j* atom along the direction α, *V* is the total volume of the system, n_d is the number of the system degrees of freedom, k_B is the Boltzmann constant, *T* is the temperature of the system. The silicene sheets were divided into elementary areas. Stresses $\sigma_{u\alpha}(l)$ arising under the action of forces of the direction $\alpha(=x, y, z)$ were calculated on every area with the *l* number and *u* orientation. When summing equation (5), only those forces, which appear from the interaction between the *i* and *j* atoms and passing through the *l* area, were taken into account.

To study the structure of the short-range order in the walls of the silicene channels under consideration, we used the method of statistical geometry. It is based on the construction of the combined polyhedra. The center of the Li^+ ion moving along the channel is recognized as the center of each polyhedron of the aforesaid construction. The nearest neighbors (forming the faces of the combined polyhedron) are Si atoms belonging to the channel walls. Polyhedra were built every 1000 time steps. Thus, the obtained statistical characteristics were based on the construction of 1000 polyhedra. The details of the method and its verification for the two-dimensional structures are given in work [7].

The roughness R_a of the doped silicene sheets was determined through the average deviation of the Si atoms *z* coordinates in the sheet relative to the location of the main *z* plane

$$R_a = \frac{1}{N}\sum_{i=1}^{N}\left|Z_i - \overline{Z}\right| \quad (6)$$

here *N* is the number of nodes (atoms) on the silicene surface, Z_i – is the displacement of the *i* atom in the direction of the 0*z* axis, $\overline{Z}$ is the average value of the z coordinate for the silicene structure; values of Z_i and $\overline{Z}$ are determined at the same moment of time [47].

The open-source LAMMPS code for parallel computing in the MD method was used [48]. All calculations were performed on a URAN cluster-type hybrid computer at the N.N. Krasovskii Institute of Mathematics and Mechanics UB RAS with a peak performance of 216 Tflop/s and 1864 CPU.

3. Results and discussions

The interactions between various elements in the model were calculated based on Morse potentials. The parameters were determined using quantum mechanical calculations. The correctness of the interactions should primarily affect such characteristics as the binding

energy E_b between Li and silicene, the barrier ΔE for the diffusion of Li over the silicene surface, and the diffusion coefficient D of Li atoms. Fig. 2 shows the binding energy (E_b) between Li^+ ion and Si atoms forming the walls of the doped silicene channel.

The binding energy between the ion and the channel walls without and with different doping degrees is in the range of $1.70 \leq E_b \leq 2.09$ eV. This value calculated for the most favorable adsorption sites for the Li atom on silicene is ~2.1 eV [49]. As the P concentration increases from 3% to 6%, the E_b decreases by 3%. With a further increase in the phosphorus concentration, the binding energy continues to decrease. It reaches minimum at the phosphorus concentration of 18%. Most likely, in systems with 3% and 6% P-doping, the Li^+ ion occupies energetically more preferable sites near the channel walls. However, when the degree of doping is 9% or 18%, the relief of the channel walls changes significantly due to the displacement of P atoms inside the channel. At the same time, the number of preferable sites for the lithium ion adsorption decreases.

We estimated the diffusion barrier of Li on perfect silicene as 0.17 eV. In quantum-mechanical calculations, the diffusion barrier of Li was found to be 0.14–0.26 eV [50].

The diffusion coefficient of lithium ions calculated through the mean square displacement of these atoms turns out to be weakly correlated with a phosphorus content in the channel walls (Fig. 3). Li ions in channel formed of pristine silicene and silicene with mono- or bivacancies have fairly close D values. The P atoms that separate from the channel walls begin to influence strongly smoothing out of the silicene buckles. Already at 6% P content in silicene, the channel walls become noticeably straighter, which leads to the increase in the D value. When doping reaches 9%, the channel straightening is further enhanced and the D coefficient reaches its maximum value. However, at 18% doping (hexavacancies were initially filled with P atoms) the value of D drops sharply due to the presence of a large number of P atoms inside the channel that interfere with the diffusion of Li^+.

The estimated value of the Li^+ diffusion coefficient in the perfect silicene channel is $1.2{\cdot}10^{-5}$ cm^2/s. A higher value of the diffusion coefficient of the Li^+ ion on the single-layer silicene was established based on the first-principles (DFT) calculations ($5.0{\cdot}10^{-5}$ cm^2/s) [18]. In turn, the values of the D_{Li}^+ coefficient in the silicene channels obtained by us are too high in comparison with the experimentally determined value of D_{Li}^+ in nano-Si (~10^{-12} $cm^2\,s^{-1}$) [51].

The first step of the calculations is associated with the study of the

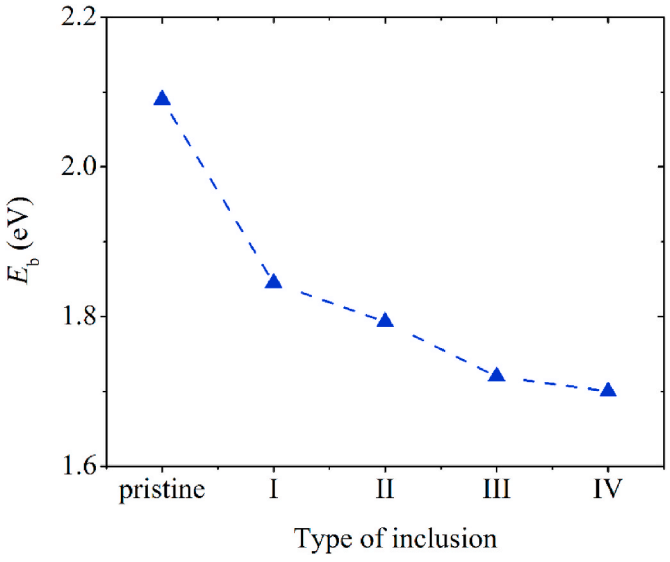

Fig. 2. Binding energy E_b of the Li atom with doped silicene as a function of phosphorous dopant; I, II, III, IV - mono-, bi-, tri- and hexavacancies in silicene, respectively.

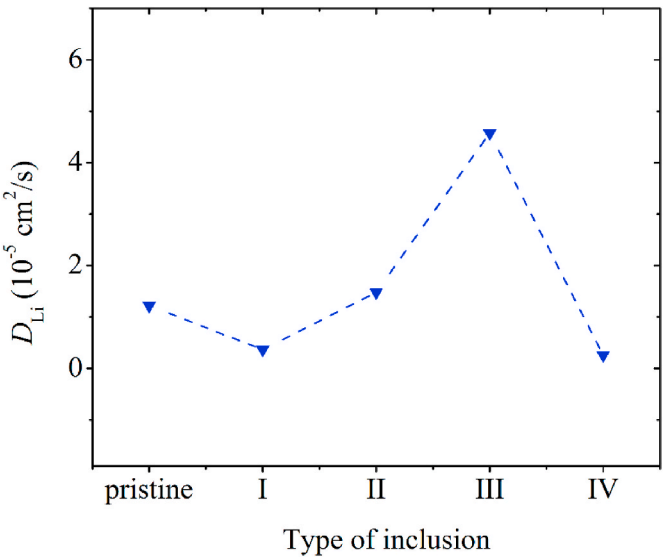

Fig. 3. Diffusion coefficient of Li ions during their movement along the pristine silicene channel and a two-layer silicene with the P atoms initial filling: I, II, III, IV - mono-, bi-, tri- and hexavacancies in silicene, respectively.

Li^+ ion motion in the 3% P-doped silicene channel with various gaps $h_g = 0.6$, 0.7, 0.75, and 0.8 nm. Fig. 4(a) shows the configuration of the system corresponding to the time moment of 100 ps, $h_g = 0.6$ nm. In this case, the Li^+ ion passes the channel along a smooth trajectory with the slight deviations to the channel walls. Due to the influence of the modified graphene substrate, the lower (adjacent to the substrate) channel wall appears to be flatter than the upper wall at the instant of time 100 ps. However, in the upper wall of the channel, the size of the buckles also decreases. The straightening of the doped silicene sheets can be explained by the influence of the impurity, i.e. P atoms. The size of the P atom is smaller than the size of the Si one. The substitution of P atoms for Si atoms results in the distance decrease between the majority of the atoms in the silicene sheet. This causes a reduction in the height of the buckles in the silicene sheet. Note that the straightening process is not associated with the loss of stability of monolayer silicene, because the elastic constants of the second order and Young's modulus for the planar silicene indicate its stability [30]. We also observed the effect of silicene straightening when modeling the motion of the Li^+ ion in the silicene channel located between two graphene sheets [43].

Fig. 4(b) shows that the silicene hexagonal structure is not preserved everywhere. The structure is rearranged in the vicinity of the locations of P atoms. The phosphorus atoms are pushed onto the sheet surface from the monovacancy where they were initially located. At the same time, each monovacancy is transformed into three adjacent 5-membered rings after 100 ps. In Fig. 4(b) they are marked with dashed circles. Such behavior of phosphorus in silicene is confirmed in quantum-mechanical calculations [8]. According to work [8], the most energetically favorable position of the P adatom in monolayer silicene is the location above the Si atom (hill site). In this case, the binding energy is maximum and equals to 5.28 eV. For comparison, when the phosphorus atom is located above the center of the hexagonal silicon ring (hollow site), the energy of the Si–P bond is 2.87 eV.

A triple of the closely spaced Si atoms in silicene sheets is formed at the points where three adjacent five-membered Si rings converge (Fig. 4 (b)). These rings are formed as a result of the disappearance of the monovacancy, in which the P atom was located. When five-membered rings appear, the P atom is located above the formed triple of the Si atoms. The Si–P bond established in the doped silicene is polarized due to the difference in the electronegativities of the Si and P atoms (1.9 and 2.1, respectively). The nature and degree of polarization of this bond in a real system are determined by electronic effects caused by the presence

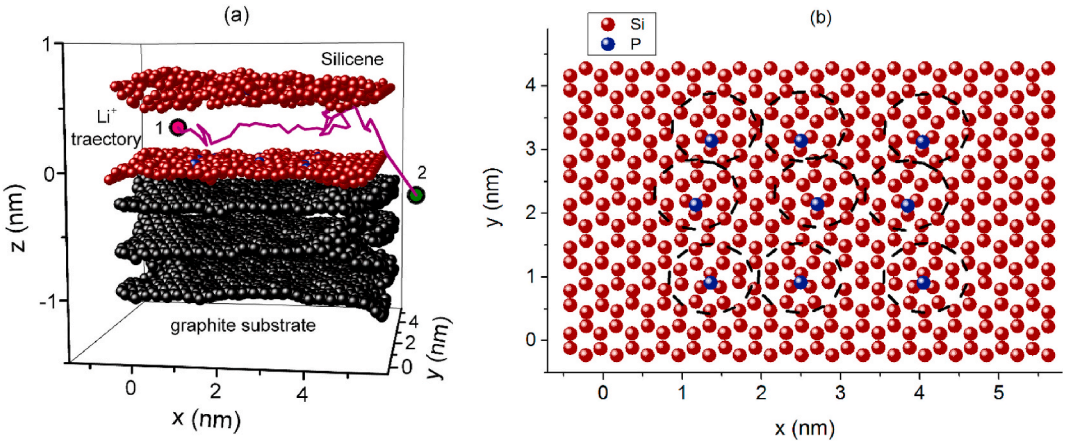

Fig. 4. (a) Configuration of the system "3% P-doped silicene channel located on the 5% N-doped graphite substrate" including the Li^+ trajectory; the gap between the silicene sheets is 0.6 nm, 1 and 2 are the initial and final points of the Li^+ trajectory; (b) *xy*-projection of the top silicene sheet of this system; dashed circles represent the transformation areas of the P-doped structure; (a) and (b) correspond to a time instant of 100 ps.

of impurities, as well as by the coordination numbers of Si and P atoms [52]. A single Si–P bond is highly reactive and cleaves easily with suitable polar compounds. Double Si=P bonds are more stable. As a result, the five-valent P atom prefers to bind with three closely spaced Si atoms rather than to attach to six Si atoms at once being located above the center of the hexagonal Si-cell.

The residence time of the Li^+ ion with a further increase in the gap size of the silicene channel is shown in Table 2. As it can be seen from Table 2, only at $h_g = 0.7$ nm the ion did not leave the channel during the observation time. The reason for that was the strong curvature of the silicene sheets. It prevented the Li^+ ion from moving through the channel. We observed the effect of strengthening the silicene sheet after doping it with phosphorus. So, in the absence of phosphorus in monovacancies, the silicene channel showed less stability when lithium ion moved along it [40].

The second step of computational experiments was carried out with a constant gap between the silicene sheets $h_g = 0.75$ nm. Such a channel gap is optimal with respect to the uniformity and completeness of the filling of the channel with lithium [43]. In the present study, Li^+ ion passes through the channel with different doping degrees of the silicene sheets: 3%, 6%, 9%, 18%. Fig. 5 shows the configurations of the system "P-doped silicene channel located on the 5% N-doped graphite substrate" with (a) 9% and (b) 18% doping. The configurations correspond to the time moment of 100 ps.

When doping by phosphorus atoms that filled trivacancies in the silicene sheets (9% doping), the lithium ion was able to leave the channel after 83 ps (Table 2). In this case, the silicene walls of the channel remained undistorted. On the contrary, when hexavacancies in silicene are doped by phosphorous atoms (18% doping), the ion "stucks" in the space between the bottom silicene sheet and the top sheet of the graphite substrate. The Li^+ ion could penetrate there through one of the holes that appeared as a result of the P atoms displacement from vacancies. In this case, the channel walls were significantly deformed. At the doping degree of 6% and 18%, the exit of the ion from the channel was not observed for the time of 100 ps (Table 2). The quantum-mechanical calculations [18] show that the Li^+ ion can move freely both along the surface of the silicene sheet and with stopping at different hollow positions (in the center of the hexagonal silicon ring). In the first case, the Li^+ ion needs to overcome an energy barrier of 0.25 eV, and in the second case, 1.2 eV. Thus, the preferred trajectory for Li^+ is the movement along the surface of the silicene sheet, which we observe in the present MD calculations when Li^+ moves in the Si channel.

The configurations of the silicene channel obtained by the time moment of 100 ps with 6% and 18% P-doping are shown in Fig. 6 in two views. The silicene sheets have a slight distortion at 6% phosphorus doping (Fig. 6(a)). Fig. 6(a) shows the formation of oval multi-membered rings instead of the bivacancies locations. In this case, P atoms adjacent to holes, which occupy locations over the triples of Si atoms, appear. In the vicinity of each P atom, 5- and 8-membered cyclic formations formed. *Ab initio* MD simulation [8] showed that the system is stable for at least 2 ps after substitution of Si atoms by P atoms. Similar behavior of bivacancies in the undoped silicene structure was confirmed by the density functional theory method [53]. The appearance of closed cyclic formations made it possible to minimize the number of dangling bonds. It is believed that the bivacancy is the most energetically preferable structural defect comparing with another vacancy defect in silicene [54]. In addition, the presence of bivacancies in planar silicene leads to the appearance of a significant magnetic moment. It is not observed in the case of silicene with monovacancies [55]. Moreover, if the bivacancies in silicene are filled with phosphorus atoms, the magnetic moment is preserved.

The front view of the channel presented in the inset of Fig. 6(a) shows a significant distortion of the channel in the area of the right edge. This circumstance, obviously, caused the stuck of the Li^+ ion in the Si channel with 6% degree of doping.

In the case of 18% doping of silicene, the significant structural rearrangements in the areas of defects location in the silicene sheets is observed. Also, the change in the channel shape is vividly seen (Fig. 6 (b)). The phosphorus atoms (that were originally inside the hexavacancies) are located along the perimeter of the hexavacancies at a time moment of 100 ps. In the inset of Fig. 6(b), the bending of the channel in its central part, that caused the stuck of the Li^+ ion in the channel, is seen. The motion of the Li^+ ion shows that the silicene sheets were already significantly distorted by the time instant of 20 ps. The

Table 2
The residence time of the lithium ion in the phosphorus-doped silicene.

Gap in the silicene channel, nm	0.6	0.7	0.75	0.8	0.75	0.75	0.75
Phosphorus concentration in the silicene sheets	3%	3%	3%	3%	6%	9%	18%
t, ps	52	the ion doesn't leave the channel	106	24	the ion doesn't leave the channel	83	the ion doesn't leave the channel

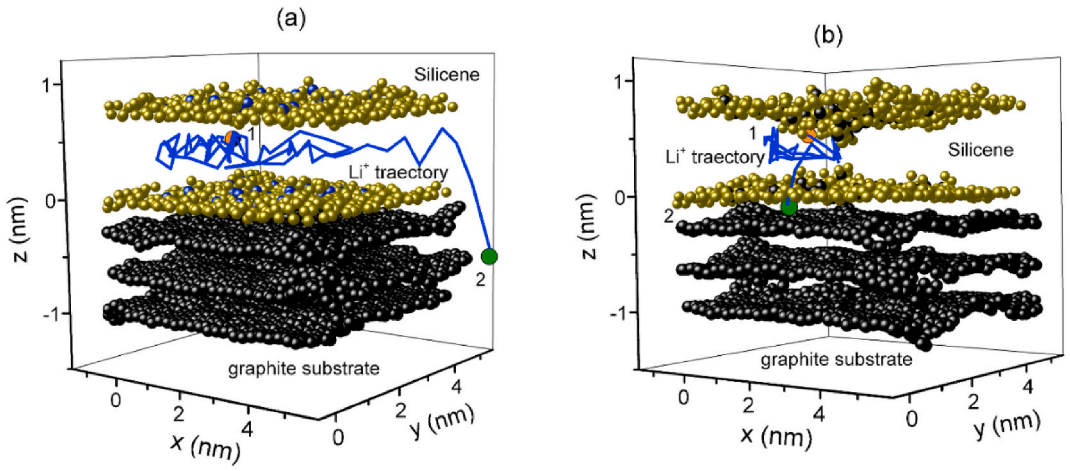

Fig. 5. Trajectories of the Li^+ ion under the external electric field in the channel formed by the P-doped silicene sheets located on the 5% N-doped graphite substrate; 1 denotes the initial and 2 denotes the final points of Li^+ trajectory; phosphorus content in the silicene sheets: (a) 9%, (b) 18%; (a) and (b) correspond to a time instant of 100 ps.

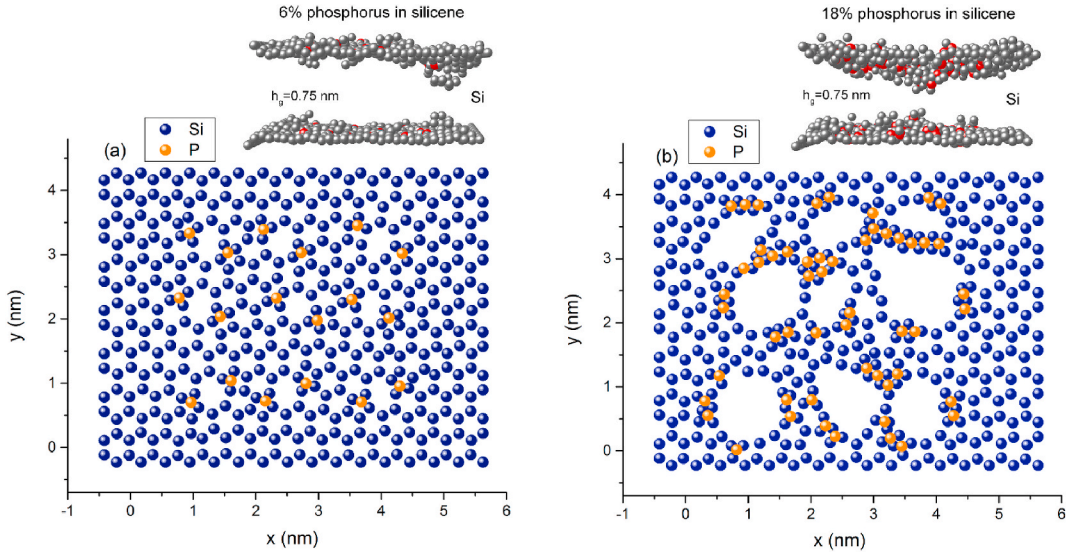

Fig. 6. *Xy*-projections of the top silicene sheets of the systems "P-doped silicene channel located on the 5% N-doped graphite substrate"; phosphorus content: (a) 6%, (b) 18%; inserts show (under small representing angle) *zx*-projections of the corresponding doped silicene channels; (a) and (b) correspond to a time instant of 100 ps.

greater is the silicene doping degree, the more difficult it is for the Li^+ ion to pass through the channel. However, on the other hand, the silicene sheets are significantly strengthened when the doping degree is up to 9% inclusive. In all systems under consideration, N-doped graphene sheets forming a graphite substrate have edge distortions but remain stable throughout the calculation time.

The horizontal and vertical stresses arising in the silicene sheets with different doping as a result of the lithium ion movement are shown in Fig. 7. Stresses in the «zig-zag» (a) and (b) and «armchair» (c) and (d) directions are comparable to each other. They do not exceed the tensile strength of silicene under the uniaxial tension (12.5 GPa) [56]. The greatest σ_{zx} stresses in the «zig-zag» direction are located at the edges of the silicene sheets. The maximum values of σ_{zy} stresses are localized in the direction of the «armchair» mainly in the central part of the silicene sheets. The σ_{zz} stresses are distributed evenly in both directions. The behavior and magnitudes of stresses in different directions in the doped silicene sheets are comparable with stresses in the perfect and defective undoped 2D Si structures located on different metal substrates (Ag, Cu, Al, Ni) [57,58].

One of the main characteristics of the statistical geometry method is the angular distribution of the nearest geometric neighbors (θ-distribution). In this study, we consider the θ angles formed by the pairs of the nearest Si neighbors and the center of the polyhedron (vertex of the angle). The obtained θ-distributions for the silicene channels under consideration are presented in Fig. 8. The dependence of the θ-distribution on the gap size of the silicene channel is shown in Fig. 8(a). The influence of the doping degree of the silicene sheets can be estimated from Fig. 8(b). The peaks in the θ-distribution show the crystallinity of the packing. The continuous spectrum suggests the presence of structural irregularity. Sharp peaks at the angles of ~30°, 60°, and 90° are present almost in all θ-distributions. Moreover, the system with 3% doped silicene sheets and the gap size of 0.75 nm has the spectrum with lots of sharp peaks. All presented θ-spectra in Fig. 8 show the presence of significant irregularity in the crystal structure of the P-doped silicene sheets. None of the peaks in these distributions are fully resolved. The obtained θ-spectra never extend to angles θ ~180°. The truncated θ-spectrum suggests that the Li^+ ion is mostly localized near one of the silicene channel walls.

In [58], the structure of silicene calculated by the DFT method could change as a result of the deposition of lithium on a silicene sheet in the

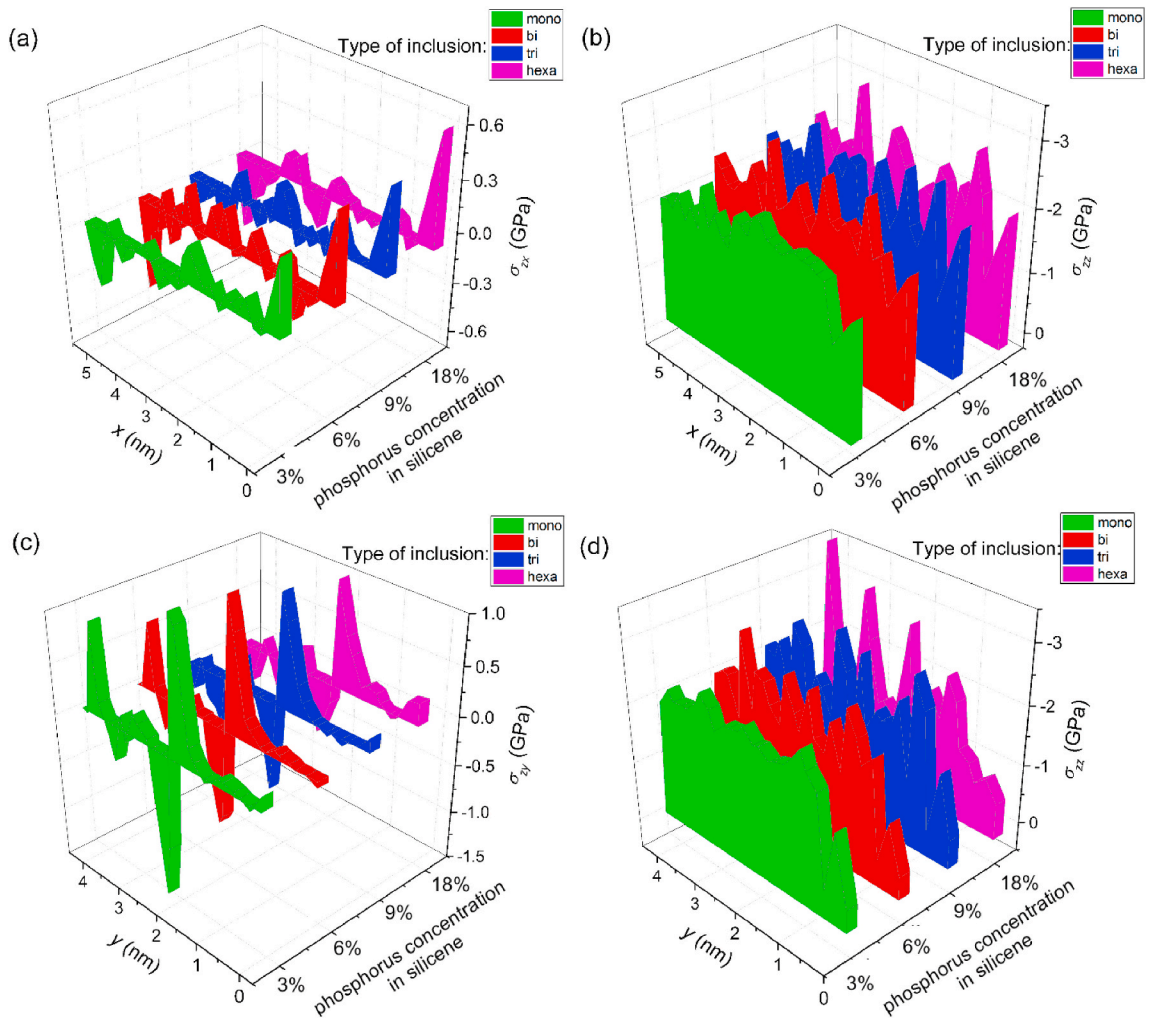

Fig. 7. Stress distribution in the bottom sheet of doped silicene channel with different phosphorous concentrations located on the 5% N-doped graphite substrate: (a) σ_{zx}, (b) σ_{zz}, (c) σ_{zy} and (d) σ_{zz}; elementary areas elongated along the direction: (a) and (b) – «zig-zag», (c) and (d) – «armchair».

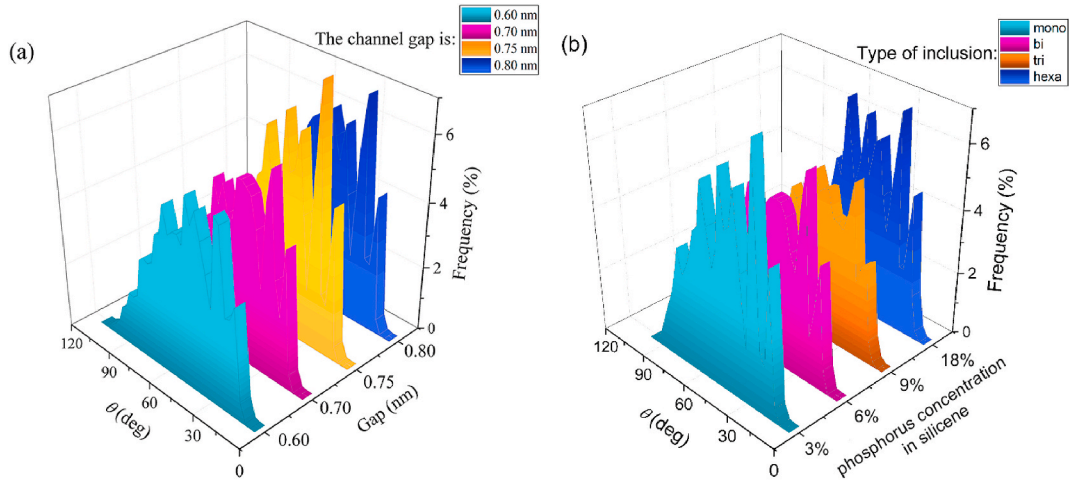

Fig. 8. Angular distribution of the nearest geometric neighbors for the P-doped silicene channel located on the 5% N-doped graphite substrate: (a) for the channels with different gaps, (b) for the channel with the gap of 0.75 nm and different phosphorus concentrations; the Li^+ ion motion along the channel during 100 ps is used as a probe.

form of atomic chains. Modulations (such as were described by S. Xu et al. [58]) of the local structure of silicene caused by the Li^+ ion passage through the channel, were not observed, probably due to the fact that the mass deposition of lithium on the channel walls was beyond the scope of the present research. As follows from Fig. 9, the silicene structure with the phosphorus content of 9% is rapidly rearranged

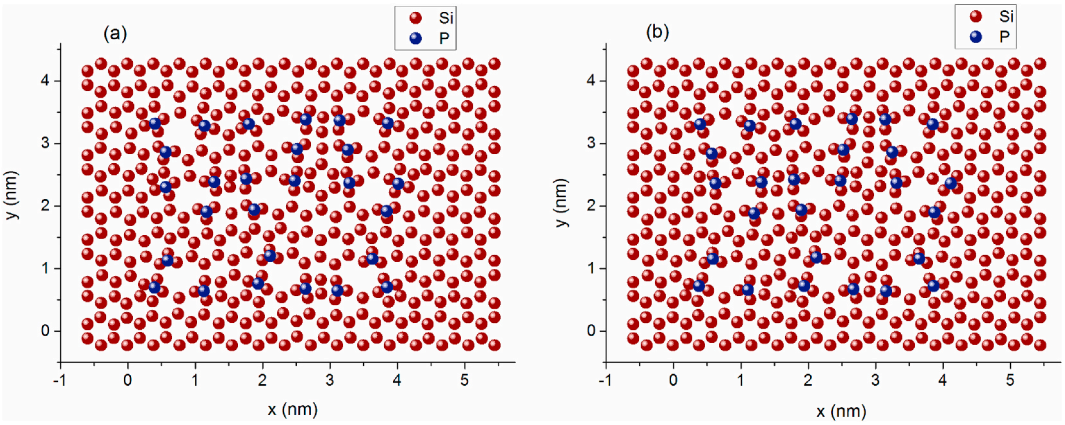

Fig. 9. *Xy*-projections of the bottom silicene sheet with the phosphorus content of 9% of the system "P-doped silicene channel located on the 5% N-doped graphite substrate" corresponding to the time instants: (a) 10 ps and (b) 100 ps.

(already after 10 ps) due to the release of P atoms from their initial sites. Then, the structure of doped silicene slowly evolves as the Li^+ ion moves along the channel. We observed a similar picture of the structural relaxation of silicene at a phosphorus concentration of 3% and 6%.

The roughness R_a of the two-dimensional Si sheets characterizes the non-flat structure of silicene [18]. The value of R_a is shown in Fig. 10 depending on the doping degree of the silicene sheets. The bottom silicene sheets have the lower buckling than the top ones. This effect can be observed visually in the inset in Fig. 10. It shows the *zx*-projection of the silicene channel with 9% P-doping (when trivacancies are filled with phosphorus). The vertical deviations of the Si atoms in the top sheet are much higher compared to the bottom sheet. This is primarily due to the stabilizing action of the graphite substrate on the bottom sheet. The channel formed from the silicene sheets with 18% P-doping has the highest roughness value. This fact proves the presence of the tendency for the destruction of the silicene channel with 18% P-doping (when phosphorus atoms fill hexavacancies).

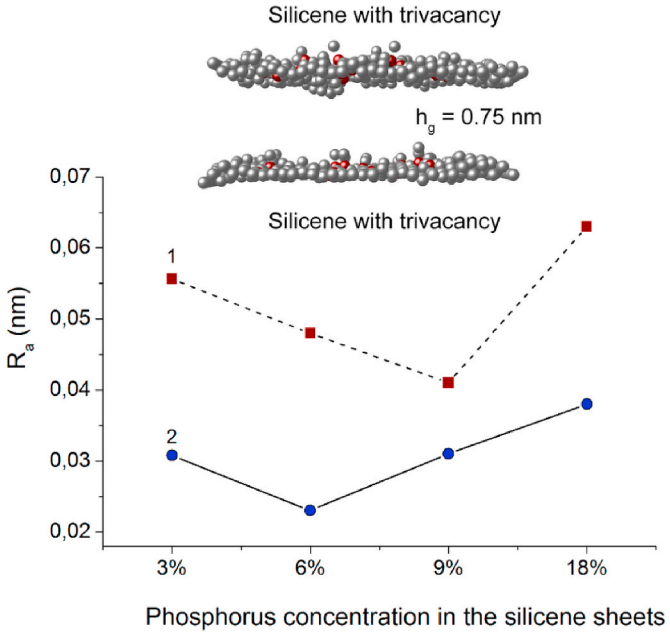

Fig. 10. Roughness of the top (1) and bottom (2) silicene sheets of the system "P-doped silicene channel located on the 5% N-doped graphite substrate" with different phosphorus concentrations; insert shows *zx*-projection of the silicene channel with the 9% phosphorus concentration.

4. Conclusion remark

The molecular dynamics method was used to study the motion of the lithium ion along the silicene channel. The Si walls of the channel were doped with phosphorus in the amount of 3%, 6%, 9%, and 18%. The channel located on the graphite substrate with 5% nitrogen doping. The gap between the sheets of the channel varied in the range of 0.6–0.8 nm. It was shown that the Li^+ ion can pass through the channel and leave it or get stuck inside it, which was found to depend both on the configuration of the channel and on the doping degree of the Si walls. By the end of the calculation (100 ps), phosphorus atoms (which initially filled mono-, bi-, tri-, and hexavacancies in silicene) were displaced onto the surface of the silicene sheets, mainly inside the channel. As a result of such a rearrangement, closed Si–Si formations appear in the places where P atoms were previously located. The silicene sheets are not destroyed during the computer experiment. The system with the silicene channel which has the 18% P-doped walls is an exception. The Li^+ ion cannot pass through such channel. There are no significant structural changes in the N-doped graphene sheets forming the N-graphite substrate.

The binding energy of lithium atoms with doped silicene continuously decreases with an increase in the phosphorus concentration in the silicene channel walls. The diffusion coefficient of lithium atoms in the channel has a complex dependence on the degree of doping of the channel walls. An increase in *D* can be associated with the straightening of the walls of the silicene channel due to P-doping. A decrease in *D* can be caused by the penetration of a significant number of P atoms into the channel.

The stresses arising in the horizontal and vertical directions are comparable for all the systems under consideration. Moreover, neither the size of the gap between the silicene channel sheets nor its doping degree affect the stresses significantly. The greatest stresses in the «zigzag» direction of the silicene sheets are located at the edges of the sheets. The maximum stresses in the «armchair» direction are observed in the central part of the Si sheets. An analysis of the structure of the sheets of the silicene channel shows the presence of a certain degree of disorder in their crystal structure. The roughness of the silicene sheets has a minimum at 9% P-doping of the top silicene sheet and at 6% P-doping of the bottom sheet. Moreover, the bottom wall of the channel is smoother in all cases due to the influence of the graphite substrate. When the phosphorus concentration is 18%, a sharp increase in roughness, that indicates a tendency for destruction of the silicene channel, is observed.

Doping silicene with phosphorus, which shortens the height of the buckles in silicene and strengthens defective silicene sheet, seems to be an important tool for to increase the performance of an anode made of this material.

Author contributions

Alexander Galashev: Conceptualization; Methodology; Supervision; Investigation; Writing - original draft. Oksana Rakhmanova: Data curation; Investigation; Software; Visualization; Writing - original draft.

Declaration of competing interest

The authors declare no known competing financial interests or personal relationships that could have appeared to influence the work reported in this paper.

Acknowledgements

This work is performed in the frame of the State Assignment number 075-03-2020-582/1 dated 18.02.2020 (the theme number 0836-2020-0037).

References

[1] T. Wang, C. Li, C. Xia, L. Yin, Y. An, S. Wei, X. Dai, Silicene/BN vdW heterostructure as an ultrafast ion diffusion anode material for Na-ion battery, Physica E 122 (2020), 114146, https://doi.org/10.1016/j.physe.2020.114146.
[2] S. Cahangirov, M. Topsakal, E. Akturk, H. Sahin, S. Ciraci, Two- and one-dimensional honeycomb structures of silicon and germanium, Phys. Rev. Lett. 102 (2009), 236804, https://doi.org/10.1103/PhysRevLett.102.236804 (1–5).
[3] B. Shojaeverdi, E. Zaminpayma, Influence of vacancy cluster on the electronic transport properties of silicene sheet, Physica E 121 (2020), 114109, https://doi.org/10.1016/j.physe.2020.114109 (1-8).
[4] C.-C. Liu, H. Jiang, Y. Yao, Low-energy effective Hamiltonian involving spin-orbit coupling in silicene and two-dimensional germanium and tin, Phys. Rev. B 84 (2011), 195430, https://doi.org/10.1103/PhysRevB.84.195430 (1–5).
[5] G.P.P. Pun, Y. Mishin, Optimized interatomic potential for silicon and its application to thermal stability of silicene, Phys. Rev. B 95 (2017), 224103, https://doi.org/10.1103/PhysRevB.95.224103 (1–5).
[6] C. Qian, Z. Li, Multilayer silicene: structure, electronics, and mechanical property, Comput. Mater. Sci. 72 (2020), 109354, https://doi.org/10.1016/j.commatsci.2019.109354 (1–8).
[7] A.E. Galashev, K.A. Ivanichkina, Numerical simulation of the structure and mechanical properties of silicene layers on graphite during the lithium ion motion, Phys. Solid State 61 (2019) 233–243, https://doi.org/10.1134/S1063783419020136.
[8] J. Sivek, H. Sahin, B. Partoens, F.M. Peeters, Adsorption and absorption of boron, nitrogen, aluminum, and phosphorus on silicene: stability and electronic and phonon properties, Phys. Rev. B 87 (2013), 085444, https://doi.org/10.1103/PhysRevB.87.085444 (1–6).
[9] S. Bourdais, G. Beaucarne, A. Slaoui, J. Poortmans, et al., Comparative study of rapid and classical thermal phosphorus diffusion on polycrystalline silicon thin films, Sol. Energy Mater. Sol. Cells 65 (2001) 487–493, https://doi.org/10.1016/S0927-0248(00)00131-8.
[10] A.N. Gorban', V.A. Gorodokin, Low-temperature diffusion of phosphorus in silicon, Sov. Phys. J. 31 (1988) 737–740, https://doi.org/10.1007/BF00895983.
[11] H.-J. Gossmann, F.C. Unterwald, H.S. Luftman, Doping of Si thin films by low-temperature molecular beam epitaxy, J. Appl. Phys. 73 (1993) 8237–8241, https://doi.org/10.1063/1.353441.
[12] G.A. Kachurin, I.E. Tyschenko, L.I. Fedina, High-temperature ion implantation in silicon, Nucl. Instrum. Methods Phys. Res. B 68 (1992) 323–330, https://doi.org/10.1016/0168-583X(92)96103-6.
[13] A. Isakov, S. Khvostov, E. Kinev, M. Laptev, et al., Neutron transmutation doping of thin silicon films electrodeposited from the KF-KCl-KI-K_2SiF_6 melt, J. Electrochem. Soc. 167 (2020), 082515, https://doi.org/10.1149/1945-7111/ab933c (1–9).
[14] C. Pochrybniak, K. Pytel, J.J. Milczarek, J. Jaroszewicz, M. Lipinski, T. Piotrowskic, Properties of neutron doped multicrystalline silicon for solar cells, Acta Phys. Pol., A 113 (2008) 1255–1265, https://doi.org/10.12693/APhysPolA.113.1255.
[15] X.D. Pi, Z.Y. Ni, Y. Liu, Z. Ruan, M. Xu, D. Yang, Density functional theory study on boron- and phosphorus-doped hydrogen-passivated silicene, PCCP 17 (2015) 4146–4151, https://doi.org/10.1039/C4CP05196C.
[16] U. Kasavajjula, C. Wang, A.J. Appleby, Nano- and bulk-silicon-based insertion anodes for lithium-ion secondary cells, J. Power Sources 163 (2007) 1003–1039, https://doi.org/10.1016/j.jpowsour.2006.09.084.
[17] M.H. Park, M.G. Kim, J. Joo, K. Kim, J. Kim, S. Ahn, Silicon nanotube battery anodes, Nano Lett. 9 (2009) 3844–3847, https://doi.org/10.1021/nl902058c.
[18] B. Mortazavi, A. Dianat, G. Cuniberti, T. Rabczuk, Application of silicene, germanene and stanene for Na or Li ion storage: a theoretical investigation, Electrochim. Acta 213 (2016) 865–870, https://doi.org/10.1016/j.electacta.2016.08.027.
[19] A.E. Galashev, K.A. Ivanichkina, Anodes for lithium-ion batteries on metal substrates, J. Electrochem. Soc. 167 (2020), 050510, https://doi.org/10.1149/1945-7111/ab717a (1–11).
[20] M.B. Bechir, A.B. Rhaiem, The sodium-ion battery: study of alternative current conduction mechanisms on the Na_3PO_4 - based solid electrolyte, Physica E 120 (2020), 114032, https://doi.org/10.1016/j.physe.2020.114032 (1-8).
[21] D.K. Das, J. Sarkar, Comparison of mechanical properties of silicene estimated using different testing procedures: a molecular dynamics study, J. Appl. Phys. 123 (2018), 044304, https://doi.org/10.1063/1.5009084 (1–6).
[22] A.E. Galashev, K.A. Ivanichkina, Nanoscale simulation of the lithium ion interaction with defective silicene, Phys. Lett. A 381 (2017) 3079–3083, https://doi.org/10.1016/j.physleta.2017.07.040.
[23] A.Y. Galashev, K.A. Ivanichkina, Computer study of atomic mechanisms of intercalation/deintercalation of Li ions in a silicene anode on an Ag (111) substrate, J. Electrochem. Soc. 165 (2018) A1788–A1796, https://doi.org/10.1149/2.0751809jes.
[24] M.R. Zachariah, C.F. Melius, Theoretical calculation of thermochemistry for molecules in the Si−P−H system, J. Phys. Chem. A 101 (1997) 913–918, https://doi.org/10.1021/jp9617377.
[25] J. Tersoff, Empirical interatomic potential for silicon with improved elastic properties, Phys. Rev. B 38 (1988) 9902–9905, https://doi.org/10.1103/PhysRevB.38.9902.
[26] J. Tersoff, Chemical order in amorphous silicon carbide, Phys. Rev. B 49 (1994) 16349–16352, https://doi.org/10.1103/PhysRevB.49.16349.
[27] A.E. Galashev, Y.P. Zaikov, R.G. Vladykin, Effect of electric field on lithium ion in silicene channel, Comput. Exp., Rus. J. Electrochem. 52 (2016) 966–974, https://doi.org/10.1134/S1023193516100049.
[28] F. Benkabou, M. Certier, H. Aourag, Elastic properties of zinc-blende GaN, AlN and InN from molecular dynamics, Mol. Simulat. 29 (2003) 201–209, https://doi.org/10.1080/0892702021000049673.
[29] J.F. Nye, Physical Properties of Crystals, Oxford University Press, Oxford, 1985.
[30] Q. Peng, X. Wen, S. De, Mechanical stabilities of silicone, RSC Adv. 3 (2013) 13772–13781, https://doi.org/10.1039/C3RA41347K.
[31] T. Siby, K.M. Ajith, Molecular dynamics simulation of the thermos-mechanical properties of monolayer graphene sheet, Procedia Mater. Sci. 5 (2014) 489–498, https://doi.org/10.1016/j.mspro.2014.07.292.
[32] R. Yu, P. Zhai, G. Li, L. Liu, Molecular dynamics simulation of the mechanical properties of single-crystal bulk Mg_2Si, J. Electron. Mater. 41 (2012) 1465–1469, https://doi.org/10.1007/s11664-012-1916-x.
[33] S.K. Das, D. Roy, S. Sengupta, Volume change in some substitutional alloys using Morse potential function, J. Phys. F Met. Phys. 7 (1977) 5–14, https://doi.org/10.1088/0305-4608/7/1/011.
[34] T.-E. Fang, J.-H. Wu, Molecular dynamics simulations on nanoindentation mechanisms of multilayered films, Comput. Mater. Sci. 43 (2008) 785–790, https://doi.org/10.1016/j.commatsci.2008.01.066.
[35] A.Y. Galashev, K.P. Katin, M.M. Maslov, Morse parameters for the interaction of metals with graphene and silicene, Phys. Lett. A. 383 (2019) 252–258, https://doi.org/10.1016/j.physleta.2018.10.025.
[36] A.E. Galashev, K.A. Ivanichkina, K.P. Katin, M.M. Maslov, Computational study of lithium intercalation in silicene channels on a carbon substrate after nuclear transmutation doping, Computation 7 (2019) 60, https://doi.org/10.3390/computation7040060 (1-16).
[37] M.K. Song, S.D. Hong, T.N. Kyoung, The structure of lithium intercalated graphite using an effective atomic charge of lithium, J. Electrochem. Soc. 148 (2001) A1159, https://doi.org/10.1149/1.1402118 (1-8).
[38] E. Pop, V. Varshney, A.K. Roy, Thermal properties of graphene: fundamentals and applications, MRS Bull. 37 (2012) 1273–1281, https://doi.org/10.1557/mrs.2012.203.
[39] E.K. Yu, D.A. Stewart, S. Tiwari, *Ab initio* study of polarizability and induced charge densities in multilayer graphene films, Phys. Rev. B 77 (2008), 195406, https://doi.org/10.1103/PhysRevB.77.195406 (1-6).
[40] O.R. Rakhmanova, A.E. Galashev, Motion of a lithium ion over a graphene-silicene channel: a computer model, Russ. J. Phys. Chem. A 91 (2017) 921–925, https://doi.org/10.1134/S003602441705020X.
[41] T.J. Rademaker, G.R.A. Akkermans, D.L. Danilov, P.H.L. Notten, On the deviation of electroneutrality in Li-ion battery electrolytes, J. Electrochem. Soc. 161 (2014) E3365–E3372, https://doi.org/10.1149/2.0411408jes.
[42] A.E. Galashev, K.A. Ivanichkina, A.S. Vorob'ev, O.R. Rakhmanova, Structure and stability of defective silicene on Ag(001) and Ag(111) substrates: a computer experiment, Phys. Solid State 59 (2017) 1242–1252, https://doi.org/10.1134/S1063783417060087.
[43] A.E. Galashev, O.R. Rakhmanova, Y.P. Zaikov, Defect silicene and graphene as applied to the anode of lithium-ion batteries: numerical experiment, Phys. Solid State 58 (2016) 1850–1857, https://doi.org/10.1134/S1063783416090146.
[44] A.Y. Galashev, Y.P. Zaikov, Molecular dynamics study of Li^+ migration through graphene membranes, Russ. J. Electrochem. 51 (2015) 867–876, https://doi.org/10.1134/S1023193515090050.
[45] A.Y. Galashev, Y.P. Zaikov, New Si–Cu and Si–Ni anode materials for lithium-ion batteries, J. Appl. Electrochem. 49 (2019) 1027–1034, https://doi.org/10.1007/s10800-019-01344-9.
[46] A.K. Subramaniyan, C.T. Sun, Continuum interpretation of virial stress in molecular simulations, Int. J. Solid Struct. 45 (2008) 4340–4346, https://doi.org/10.1016/j.ijsolstr.2008.03.016.
[47] A.E. Galashev, O.R. Rakhmanova, K.A. Ivanichkina, Graphene and graphite supports for silicene stabilization: a computation study, J. Struct. Chem. 59 (2018) 877–883, https://doi.org/10.1134/S0022476618040194.
[48] S. Plimpton, Fast parallel algorithms for short-range molecular dynamics, J. Comput. Phys. 117 (1995) 1–19, https://doi.org/10.1006/jcph.1995.1039.

[49] G.A. Tritsaris, E. Kaxiras, S. Meng, E. Wang, Adsorption and diffusion of lithium on layered silicon for Li-Ion storage, Nano Lett. 13 (2013) 2258–2263, https://doi.org/10.1021/nl400830u.
[50] J. Deng, J.Z. Liu, N.V. Medhekar, Enhanced lithium adsorption and diffusion on silicene nanoribbons, RSC Adv. 3 (2013) 20338–20344, https://doi.org/10.1039/C3RA43326A.
[51] N. Ding, J. Xu, Y. Yao, G. Wegner, X. Fang, C. Chen, I. Lieberwirth, Determination of the diffusion coefficient of lithium ions in nano-Si, Solid State Ionics 180 (2009) 222–225, https://doi.org/10.1016/j.ssi.2008.12.015.
[52] V. Nesterov, N.C. Breit, Advances in phosphasilene chemistry, Chem. Eur J. 23 (2017) 12014–12039, https://doi.org/10.1002/chem.201700829.
[53] G.R. Berdiyorov, F.M. Peeters, Influence of vacancy defects on the thermal stability of silicene: a reactive molecular dynamics study, RSC Adv. 4 (2014) 1133–1137, https://doi.org/10.1039/C3RA43487G.
[54] S. Li, Y. Wu, Y. Tu, Defects in silicene: vacancy clusters, extended line defects and di-adatoms, Sci. Rep. 5 (2015) 7881, https://doi.org/10.1038/srep07881 (1-7).
[55] A. Majumdar, S. Chowdhury, P. Nath, D. Jana, Defect induced magnetism in planar silicene: a first principles study, RSC Adv. 4 (2014) 32221–32227, https://doi.org/10.1039/C4RA04174G.
[56] Q.-X. Pei, Z.-D. Sha, Y.-Y. Zhang, Y.-W. Zhang, Effects of temperature and strain rate on the mechanical properties of silicene, J. Appl. Phys. 115 (2014), 023519, https://doi.org/10.1063/1.4861736 (1-7).
[57] A.Y. Galashev, K.A. Ivanichkina, Computer test of a new silicene anode for lithium-ion batteries, ChemElectroChem 6 (2019) 1525–1535, https://doi.org/10.1002/celc.201900119.
[58] S. Xu, X. Fan, J. Liu, D.J. Singh, Q. Jiang, W. Zheng, Adsorption of Li on single-layer silicene for anodes of Li-ion batteries, Phys. Chem. Chem. Phys. 20 (2018) 8887–8896, https://doi.org/10.1039/C7CP08036K.